RSC Advances

ROYAL SOCIETY OF CHEMISTRY

PAPER

View Article Online
View Journal | View Issue

Cite this: *RSC Adv.*, 2021, **11**, 19813

Controllable preparation of sea urchin-like Au NPs as a SERS substrate for highly sensitive detection of the toxic atropine†

Yazhou Qin, Yuanzhao Wu, Binjie Wang, Jiye Wang, Xingsen Zong and Weixuan Yao *

Branched Au nanoparticles (Au NPs) can significantly enhance the Raman signal of trace chemical substances, and have attracted the interest of researchers. However, there are still challenges to accurately prepare the morphology of branched Au NPs. In this work, we have successfully prepared sea urchin-like Au NPs and Au nanowires by using the seed-mediate growth method, with cetyltrimethylammonium bromide (CTAB) and glutathione as ligands, and ascorbic acid as a reducing agent. Using Au NPs with a tetrahexahedron (THH) morphology as seeds, and by simply changing the concentration of glutathione, we explored the growth process of sea urchin-like Au and Au nanowires. At low concentrations of glutathione, Au NPs will preferentially grow along the edges and corners of the THH Au seed, forming a core/satellite structure. As the concentration of glutathione increases, Au NPs will grow along the direction of glutathione, forming sea urchin-like Au NPs. To further increase the concentration of glutathione, we will prepare Au nanowires. In addition, we use the prepared Au NPs as a substrate material for surface-enhanced Raman (SERS) high-sensitivity detection. By using 4-aminothiophenol (4-ATP) as the test molecule, we evaluated the SERS effect of the prepared Au NPs with different morphologies. The results showed that sea urchin-like Au NPs have the best enhancement effect. The lowest concentrations of Rhodamine 6G and 4-ATP were 10^{-10} M and 10^{-12} M, respectively, using sea urchin Au NPs as the base material. Furthermore, we conducted a highly sensitive SERS detection of the poison atropine monohydrate, and the lowest detected concentration was 10^{-10} M.

Received 25th April 2021
Accepted 26th May 2021

DOI: 10.1039/d1ra03223b

rsc.li/rsc-advances

1 Introduction

Noble metal nanomaterial are widely used in the fields of catalysis, biomedicine and optical sensing due to their excellent physical and chemical properties.[1–5] In particular, Au nanoparticles (Au NPs) have attracted great interest of researchers as a unique size and shape-dependent optical functional materials. In the past few decades, a lot of research has been devoted to the preparation of Au NPs with controllable morphology and size. Including wet chemistry,[6–8] electrochemistry,[9,10] and photochemistry[11] have been developed to prepare Au NPs of various morphology and size. In the past few decades, Au cubes,[12,13] octahedron[14,15] and rhombic dodecahedra[16,17] with low-index facet and trisoctahedral,[18,19] truncated ditetragonal,[20] tetrahexahedral,[21] hexoctahedron[22,23] and trapezohedral[24] with high-index facet have been successfully prepared. In addition, Au NPs with hierarchical structures have also been prepared, such as flower like nanoparticles,[25,26] thorn-shaped nanoparticles[27,28] and sea urchin-like nanoparticles.[29–33]

Among the various Au NPs with different morphology, the sea urchin-like Au NP is a multi-pod Au nanostructure with sharp thorns on the surface. These sharp thorns on the surface make sea urchin-like Au NPs have broader light absorption and scattering properties than spherical Au NPs of the same size. In addition, this also makes sea urchin-like Au NPs have excellent local electromagnetic field enhancement properties. The tip of the surface thorn has a strong electric field enhancement effect, which makes sea urchin-like Au NPs an excellent SERS substrate. Such tips, edges and nano-gap with electric field enhancement effect are usually called "hot spots". When analytic molecule touches the hot spot on the surface of the Au nanoparticle, its Raman signal can be enhanced by several orders of magnitude. Many studies have reported the use of sea urchin-like Au NPs as an enhanced substrate material for SERS detection. For example, Mathew and coworkers used 1,2-phenylenediamine as a template to prepare sea urchin-like Au NPs, which increased the SERS signal of crystal violet by 80 times.[34] Xu reported a method for preparing high-yield sea urchin-like Au NPs. By regulating the growth time of seed, the ratio of precursors in silver/Au seed and the amount of Au precursors

Key Laboratory of Drug Prevention and Control Technology of Zhejiang Province, Zhejiang Police College, 555 Binwen Road, Binjiang District, Hangzhou 310053, Zhejiang Province, P. R. China. E-mail: yaoweixuan@zjjcxy.cn

† Electronic supplementary information (ESI) available. See DOI: 10.1039/d1ra03223b

used for spike growth, the morphology of sea urchin-like Au NPs can be adjusted, thereby realizing highly sensitive detection of 4-mercaptobenzoic acid.[35] Li *et al.* used sea urchin-like Au NPs combined with graphene aerogel to detect tumor DNA in human blood.[36] In recent years, a lot of research has been devoted to the controllable preparation of sea urchin-like gold nanoparticles. For example, Hsu[37] *et al.* improved the method of preparing sea urchin-like gold nanoparticles without surfactants on the basis of Vo Dinh.[38] By reducing the silver concentration from 5 μM to 2 μM, the surface branching of sea urchin-like gold nanoparticles was reduced, and a better SERS enhancement effect was obtained. Fang *et al.* prepared an array of thorn-like gold by electrochemical methods to achieve highly sensitive SERS detection (the detection limits for crystal violet and R6G are up to 10^{-10} M and 10^{-11} M, respectively), and have excellent surface-enhanced Raman spectroscopy molecular consistency (relative standard deviation of 7.17%).[39] Recently, Wang[40] *et al.* realized the regulation of the length and density of sea urchin-like gold surface branches by regulating the concentration of gold seeds, surfactants and precursors. They proposed a possible reaction mechanism for long-chain amines to partially reduce $HAuCl_4$ to Au^+. Au^+ is further combined with long-chain amines, and then assembled into micelles through aurophilic bonding or hydrogen bonding. Finally, the micelles adhere to the gold seed surface as a result. The template guides the formation of Au^0 dendrites under the action of ascorbic acid. However, achieving precise control of the complex structure of the rough surface of nanoparticles is remains a challenge.

Tripod alkaloid atropine exists in mandala, a common Chinese herbal medicine, and is often used in the rescue of organophosphorus pesticide poisoning. But atropine has the effect of anti-acetylcholine, make smooth muscle slow, inhibit gland secretion, paralyze the nerve. It has an exciting effect on the central nervous system, makes blood vessels dilate, breathing difficulties, and has greater toxicity. It is widely used for detection by high performance liquid chromatography and gas chromatography mass spectrometry. The tropane alkaloids are metabolized quickly in the body, so it is necessary to develop a rapid, highly sensitive detection technology.

In this article, we used the seed growth method to prepare sea urchin-like Au NPs and explored its growth mechanism. The experimental results show that the concentration of glutathione plays a crucial role in the morphology of Au NPs. Finally, we use R6G as the Raman reporter to explore the SERS enhancement effect of the prepared Au NPs with different morphology. Furthermore, we take advantage of the non-destructive, fast and highly sensitive of the SERS detection technology and the prepared sea urchin-like Au NPs are selected as the substrate material, achieved the trace detection of atropine. The lowest detection concentration reached at 10^{-12} M.

2 Materials and methods

2.1. Materials

Hydrochloroauric acid trihydrate ($HAuCl_4 \cdot 3H_2O$, 99.9% trace metals basis), silver nitrate (AR, 99.8%) silver acetate ($AgNO_3$, AR, 99.5%) atropine sulfate monohydrate (98.5%), anhydrous ethylene glycol (EG, 99%), poly(diallyldimethylammonium) chloride (PDDA, M_w = 400 000–500 000 D, 20 wt% in H_2O, 99%), hexadecyl trimethyl ammonium bromide (CTAB, AR, 99%), Rhodamine 6G (R6G, AR, 99%), nitric acid (HNO_3, AR) hydrochloric acid (HCl, AR), glutathione (M_w = 307.32, ≥98%) was purchased from Aladdin. The chemical reagents used in the experiment were purchased and used directly without further purification. The solutions were prepared from super pure water (18 MΩ cm) purified through a Milli-Q Lab system (Nihon Millipore Ltd.). All glassware used in the experiment was immersed in a bath of freshly prepared *aqua regia* (HCl : HNO_3 = 3 : 1) for 30 min, and rinsed twice with deionized water (18.2 MΩ cm) and ethanol.

2.2. Instruments

The morphology and structures of sea urchin-like Au NPs were studied using a field emission scanning electron microscope (SEM, 3.0 kV, SU70, Hitachi, Japan), SEM studies were performed on a JEOL JSM-6700F SEM operating at 3.0 kV. Transmission electron microscopy (TEM) was performed by a Hitachi HT7700 operated under 100 kV. High-resolution TEM and (HRTEM) were taken by a JEOL JEM-2100F operated under 200 kV. The surface-enhanced Raman spectroscopy was performed using a Raman spectrometer (Horiba HR Evolution 800) with laser excitation at 633 nm.

2.3. Synthesis of Au seed

In this article, two types of Au seed are used to prepare sea urchin-like Au NPs, which are octahedral Au NPs with low-index facet {111} and tetrahexahedral (THH) Au NPs with high-index facet {210}. The THH Au NPs with a size of about 100 nm, which was prepared according to our previous reported method with a little modified.[6] First, add 0.4 mL of poly(-diallyldimethylammonium)chloride (PDDA) to a 50 mL round bottom flask with 19 mL of ethylene glycol, and stir vigorously at 25 °C for 5 min. Then add 100 μL of 0.25 M $HAuCl_4 \cdot 3H_2O$ solution and 50 μL of 25 mM $AgNO_3$ solution to the above solution. Finally, the uniformly mixed solution was placed in an oil bath at 195 °C to react for 60 minutes. After the reaction, it was cooled to 25 °C, and the product was centrifuged at 12 000 rpm to remove the supernatant. The product was washed twice with water and ethanol, and finally the product was dispersed in 1 mM hexadecyl trimethyl ammonium bromide (CTAB) solution for later use. The preparation method of octahedral Au seed is the same as above except that $AgNO_3$ is not added.

2.4. Synthesis of sea urchin-like Au NPs

First add 200 μL of 10 mM $HAuCl_4 \cdot 3H_2O$ solution into a 20 mL glass bottle containing 4 mL of water, the solution is bright yellow. Then adds 0.8 mL of 0.1 M hexadecyl trimethyl ammonium bromide (CTAB) solution, and magnetically stir for 10 minutes at 25 °C, the solution changed from bright yellow to dark yellow. Then, 0.475 μL of 0.1 M ascorbic acid (AA) solution was added to the above solution. The color of the solution

changed from dark yellow to colorless, indicating that Au^{3+} was reduced to Au^{+}. Then, 200 μL of Au seed and glutathione were added to the above solution, and the reaction was stirred at 25 °C for 2 hours. After the reaction, it was collected by centrifugation at 5000 rpm, and washed twice with water and ethanol respectively. When investigating the effect of Au seed morphology on the reaction, Au seed with octahedral and THH morphology was added without changing the above reaction conditions. In order to explore the effect of glutathione on the growth of Au NPs, we added 2 mM glutathione 10 μL, 50 μL, 75 μL, 100 μL, 125 μL and 150 μL to the reaction system without changing other reaction conditions.

2.5. SERS characterization

First, 20 μL gold nanoparticles and 50 μL analyte were added to a 1.5 mL centrifuge tube and kept at room temperature for 30 min. Then the analyte was adsorbed on the gold nanoparticles. Drop 10 μL of the mixture onto the pre-cleaned slides and dry at 25 °C. A laser Raman spectrometer (Thermo Fisher DXR2XI) equipped with microscope (50× objective lens) and CCD detector was used to record SERS spectra. The laser wavelength was 633 nm, the laser power was 6.0 mW, and the spectra of each sample were repeated at least 5 times in 10 s accumulation time. The assignments of the Raman peak were analyzed using the accompanying software.

3 Results and discussion

Prepared Au seed with Au octahedral and THH morphology has uniform size and morphology. The corresponding SEM images are shown in Fig. S1 and S2.† The edge length of the prepared Au octahedral is about 80 nm, while the edge length of prepared Au NPs with THH morphology is about 100 nm. Fig. 1 shows the SEM image of Au crystal prepared when different amounts of glutathione are added, and the Fig. 2 is the corresponding TEM image. As shown in Fig. 1A and 2A, when 10 μL of glutathione is added, the Au crystal preferentially grows at the corners of THH Au seed. Fig. S4 and S5† are SEM images of gold nanoparticles prepared when the amount of glutathione is 10 μL and 25 μL. The high magnification SEM image further proves that when there is less glutathione, the gold nanoparticles preferentially grow on the corners of the THH gold seeds. This is consistent with previous reports.[8] When we increased the amount of glutathione to 50 μL, prepared Au nanocrystal morphology was shown in Fig. 1B and 2B. From the image, we can see that the Au crystal has grown a few thorn-like structures on the original structure. According to the TEM image (Fig. 2B), we can see that there are only 1–2 gold thorns growing on the surface of each gold seed. Keeping other reaction conditions unchanged, continue to increase the amount of glutathione, we found that the number of thorns in the prepared Au crystal gradually increased. Fig. 1C is the SEM image of Au crystal prepared when the amount of glutathione added is 75 μL, and Fig. 2C is the corresponding TEM image. Compared to Fig. 2B, we can see a significant increase in the number of thorns on the Au crystal. From Fig. 2C, we can see that the number of gold thorns on the surface of each particle is about 10. When glutathione is further increased to 100 μL, we will get sea urchin-like Au crystal as shown in Fig. 1D. From the corresponding TEM micrograph (Fig. 2D), we can see that the number of thorns on the Au crystal

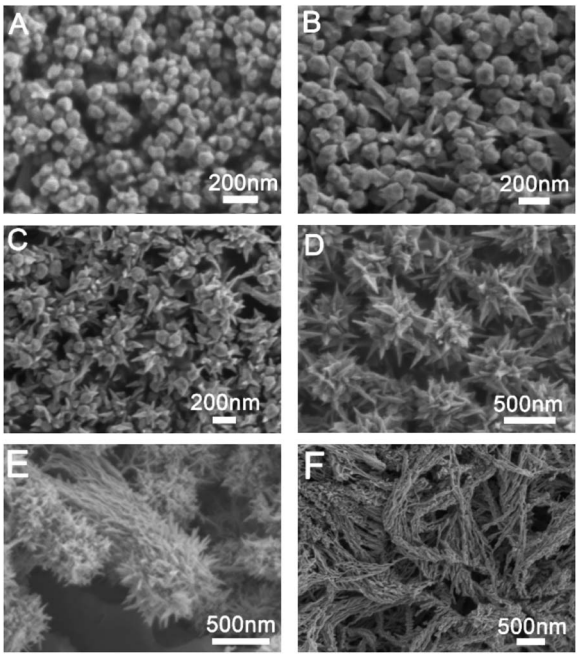

Fig. 1 SEM images of gold nanostructures prepared under different amount of glutathione in the growth solution; (A) 10 μL, (B) 50 μL, (C) 75 μL, (D) 100 μL, (E) 125 μL and (F) 150 μL.

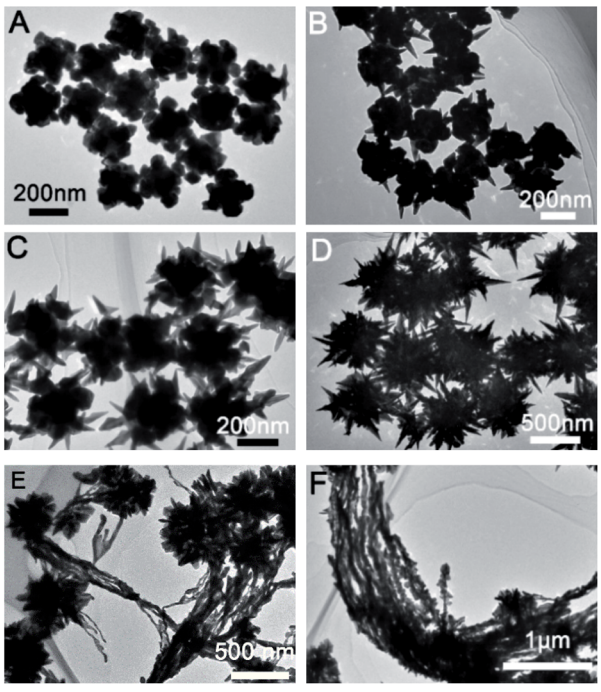

Fig. 2 TEM images of gold nanostructures prepared under different amount of glutathione in the growth solution; (A) 10 μL, (B) 50 μL, (C) 75 μL, (D) 100 μL, (E) 125 μL and (F) 150 μL.

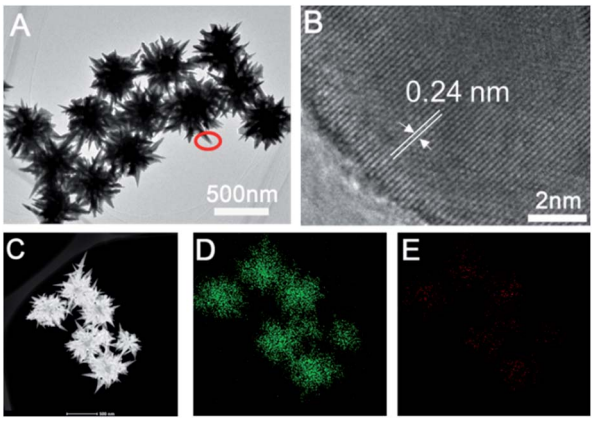

Fig. 3 Characterization of sea urchin-like gold crystals. (A) TEM image of Au crystal. (B) HRTEM image of Au crystals (C) HADDF-STEM image of gold crystals. (D) and (E) EDS elemental mapping of Au crystals indicating the Au and S elemental distribution.

has further increased, forming a sea urchin-like structure with densely distributed Au thorns. Interestingly, when we further increased glutathione to 125 μL, in addition to the sea urchin-like morphology, we also got sea urchin-like gold nanoparticles with tails (Fig. 1E and 2E). From the SEM and TEM images, we can see that strip-shaped Au nanocrystal have grown on one side of the original sea urchin-shaped Au NPs. When adding 150 μL glutathione, we will get willow-like Au nanocrystal, as shown in Fig. 1F and 2F. From the TEM image (Fig. 2F), we can see that each strip-shaped Au nanocrystal is covered with small Au NPs.

Furthermore, we further characterized the prepared sea urchin-like Au crystal and willow-like Au crystal, as shown in Fig. 3 and 4. From the TEM image of sea urchin-like Au NPs (Fig. 3A), we can see that the sea urchin-like Au NPs have uniform size and morphology. The size of sea urchin-like Au NPs is about 500 nm and has sharp thorns distributed on the surface. The HRTEM image (Fig. 3B) recorded from the circled area in Fig. 3A is used to further observe the structure of the synthesized sea urchin-like Au crystal. As shown in Fig. 3B, the lattice spacing is 0.24 nm, which indicating the thorns of Au nanostructure are mainly composed of {111} planes. And Au crystal was further identified by high-angle annular dark field scanning transmission electron microscopy (HAADF-STEM) as shown in Fig. 3C and energy dispersive X-ray spectroscopy (EDS) elemental mapping (Fig. 3D and E). From the EDS spectrum of sea urchin-like Au NPs, we can see that a small amount of S is distributed on the Au nanoparticles. Similarly, prepared willow-like Au crystal were further characterized (Fig. 4). Fig. 4A is TEM image of willow-like Au particles, we can see that the willow-like Au surface is not smooth, but covered with thorn-like particles. The HRTEM characterization of the willow-like Au particles shows that the lattice spacing is 0.24 nm (Fig. 4B), which is consistent with the results of the sea urchin-shaped Au NPs. And the HAADF-STEM image of willow-like Au particles was shown in Fig. 4C. The EDS results of the willow-shaped Au particles also show that S is distributed on the Au nanoparticles (Fig. 4D and E), which is consistent with the sea urchin-like Au particles.

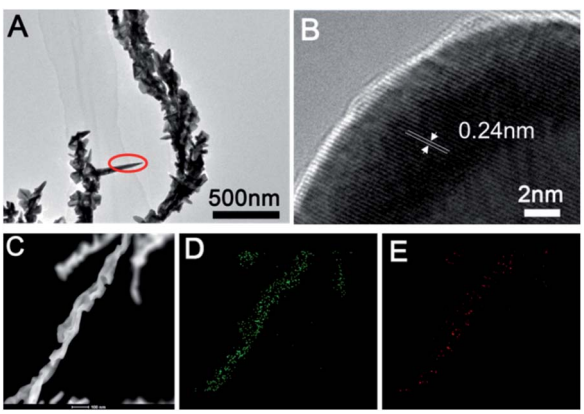

Fig. 4 Characterization of willow-like gold crystals. (A) TEM image of Au crystal. (B) HRTEM image of Au crystals (C) HADDF-STEM image of gold crystals. (D) and (E) EDS elemental mapping of willow-like Au crystals indicating the Au and S elemental distribution.

Moreover, we further explored the influence of Au seed morphology on the growth process of Au. Without changing other reaction conditions, we replaced the THH Au seed with 80 nm Au octahedral for reaction. As shown in Fig. S3,† when 200 μL of Au seed and 40 μL of 2 mM glutathione were added, we also prepared sea urchin-like Au NPs. Based on the above experimental phenomena, we have made the following inferences on the growth mechanism of Au NPs. First, when CTAB is added to the $[AuCl_4]^-$ solution, the solution turns from bright yellow to dark yellow, indicating that Au^{3+} combines with Br^- in CTAB to form a complex $[AuBr_4]^-$. The solution changed from dark yellow to colorless after adding AA, indicating that Au^{3+} is reduced to Au^+ under the action of the reducing agent AA. Glutathione is modified to the surface of Au seed through Au–S bonds.[41,42] When Au seed modified with glutathione is added, Au^+ binds to glutathione and is subsequently reduced to Au^0. The reduced Au^0 is preferentially deposited at the higher energy sites (corners) of the Au seeds (Fig. S4 and S5†). This process is consistent with previous reports.[8] As the concentration of glutathione increases, we infer that it will be assembled on the surface of gold seeds through chemical bonds or hydrogen bonds, and Au^+ will be reduced to Au^0 *in situ*, so gold nanoparticles will grow along the direction of glutathione and finally forms sea urchin-like Au NPs. Too high a concentration of glutathione promotes the growth of Au crystal into strips.

Taking 4-ATP as the target molecule, we further explored the SERS enhanced effect of the prepared Au NPs with different morphology. The Au NPs with different morphology were mixed with 4-ATP of 10^{-6} M, and then stood for 30 min at room temperature, so that 4-ATP was adsorbed on the surface of the Au NPs by Au–S bond. The nanoparticles were then dried at 25 degrees for Raman tests. As shown in Fig. 5, we can see that the enhancement effect of Au NPs from high to low is sea urchin-like, a small amount of spiny, THH morphology and wicker-like. Two distinct characteristic peaks located at 1085 cm^{-1} and 1595 cm^{-1} correspond to the C–C and C–S bond vibrations

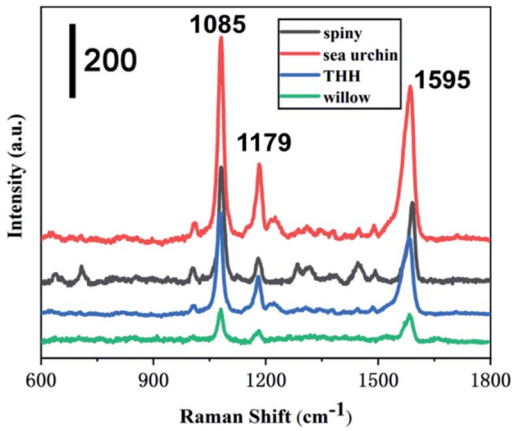

Fig. 5 Raman spectra of willow-like Au NPs (green), gold nanoparticles with THH morphology (blue), small amount of spiny gold nanoparticles (black) and sea urchin-like gold nanoparticles (red) covered substrates.

in the 4-ATP molecule, respectively. We further used sea urchin-like Au NPs to detect different concentrations of 4-ATP, R6G and the poison atropine sulfate monohydrate. Fig. 6A is the SERS spectrum of R6G, the peaks are located at 612 cm^{-1} (C–C–C in-plane bending), 773 cm^{-1} (C–H out-of-plane bending), 1181 cm^{-1} (C–H in-plane bending), and 1311 cm^{-1} (C–O–C stretching), and 1361, 1508, 1572, and 1649 cm^{-1} are the C–C stretching mode peaks of the aromatic ring. The lowest detectable concentration of R6G is 10^{-10} M. Fig. 3B shows the SERS spectra of 4-ATP molecules with different concentrations. We can see that the lowest detectable concentration of 4-ATP molecules is 10^{-12} M. Fig. 3C shows the SERS spectra of 10^{-8} M 4-ATP collected from 20 randomly selected positions. In addition, we further calculated the relative standard deviation (RSD) value. Specifically, the standard deviation of the intensity of the peak at 1085 cm^{-1} of the selected spot was 7.3% (Fig. 6D), indicating a small change, thus confirming the good reproducibility of the SERS substrate.

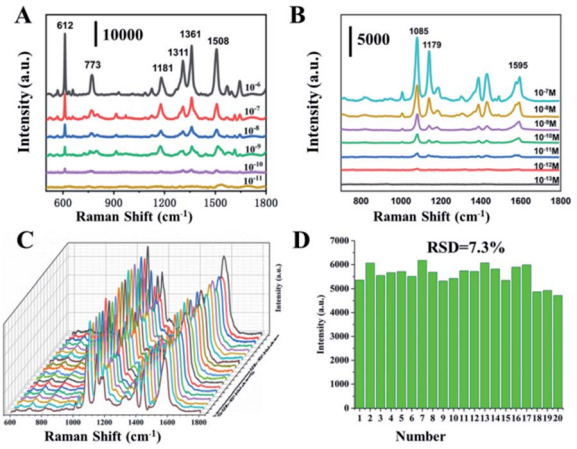

Fig. 6 (A) SERS spectra of R6G at different concentrations, (B) SERS spectra of 4-ATP molecules at different concentrations, (C) SERS spectra of 20 different points of 4-ATP. (D) Graphs of the intensity of the peaks at 1085 cm^{-1} from 20 SERS spectra.

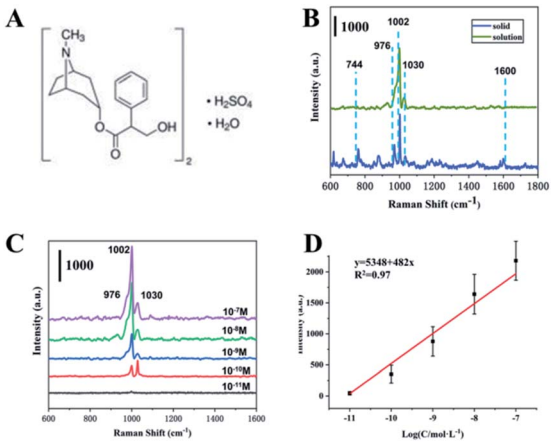

Fig. 7 (A) Molecular structures of atropine sulphate monohydrate, (B) Raman spectrum and SERS spectrum of atropine sulphate monohydrate powders, (C) SERS spectra of atropine sulphate monohydrate at different concentrations, (D) intensity of 1002 cm^{-1} as a function of the concentrations of atropine sulphate monohydrate.

Furthermore, we tested the cholinergic drug atropine sulfate. First, routine Raman detection was performed on atropine sulphate powder. The structure of atropine sulphate monohydrate is shown in Fig. 7A. As shown in Fig. 7B (blue line), Raman peaks of powdered atropine are located at 744 cm^{-1}, 877 cm^{-1}, 976 cm^{-1}, 1002 cm^{-1}, 1030 cm^{-1} and 1450 cm^{-1}. However, the SERS spectrum of the atropine solution only shown three peaks (green lines) of 976 cm^{-1}, 1002 cm^{-1} and 1030 cm^{-1}, corresponding to the symmetrical in-plane stretching vibration of the benzene ring + C–C–O swinging stretching vibration and C–C–O stretching vibration + benzene ring breathing vibration and benzene ring in-plane symmetric stretching vibration + N heterocyclic symmetric stretching vibration. Generally, for a group, the Raman peak of tensile vibration usually appears in the higher frequency range of the frequency spectrum, and is less affected by the external environment. The Raman peak of deformation vibration is usually located in a lower frequency range and is sensitive to environmental changes.[43] The peak at 744 cm^{-1} is the swing vibration of the CH_2 group in the aliphatic ring, which is easily affected by the SERS detection environment and disappears. As shown in Fig. 7C, as the concentration of atropine sulfate decreases, the intensity of its Raman peak gradually decreases, and the lowest detected concentration is 10^{-10} M. The strongest signal at 1002 cm^{-1} comes from a benzene ring breathing vibration, which was chosen to establish a relationship between signal strength and the logarithm of molecular concentration, as shown in Fig. 7D. For concentration-dependent SERS intensity, the R^2 obtained by linear fitting was 0.97. It shows that the prepared SERS substrate material has excellent enhancement effect and stable detection performance.

4 Conclusions

In summary, we used the seed growth method and glutathione as the ligand to prepare sea urchin-like and strip-like Au NPs. The growth mechanism was explored by systematically

exploring the influence of reaction conditions. More, with 4-ATP as the target molecule, we explored the SERS enhancement effect of Au NPs with different morphology, and the results shown that sea urchin-like Au NPs have excellent enhancement effects. We will prepare sea urchin-like Au NPs as the SERS substrate material for the detection of 4-ATP, R6G and the poisonous atropine sulfate, with the lowest detection concentrations of 10^{-12} M, 10^{-10} M and 10^{-10} M. This work not only provides a method for preparing sea urchin-like Au NPs also provides guidance for the development of highly sensitive SERS substrates.

Conflicts of interest

There are no conflicts to declare.

Acknowledgements

This work was supported by the National Key Research and Development Program of China Public Safety Risk Prevention and Control (2018YFC0807201) and Basic Public Welfare Research Program of Zhejiang Province (LGF20C090001).

Notes and references

1 Y. Cao, R. Jin and C. A. Mirkin, *Science*, 2002, **297**, 1536.
2 J. Fang, S. Du, S. Lebedkin, Z. Li, R. Kruk, M. Kappes and H. Hahn, *Nano Lett.*, 2010, **10**, 5006.
3 Z. Liu, L. Cheng, L. Zhang, Z. Yang, Z. Liu and J. Fang, *Biomaterials*, 2104, **35**, 4099–4107.
4 K. Saha, S. S. Agasti, C. Kim, X. Li and V. M. Rotello, *Chem. Rev.*, 2012, **112**, 2739.
5 Y. Qin, Y. Lu, W. Pan, D. Yu and J. Zhou, *RSC Adv.*, 2019, **9**, 10314.
6 Y. Qin, Y. Lu, D. Yu and J. Zhou, *CrystEngComm*, 2019, **21**, 5602–5609.
7 Y. Qin, W. Pan, D. Yu, Y. Lu, W. Wu and J. Zhou, *Chem. Commun.*, 2018, **54**, 3411–3414.
8 H. Lee, H. Y. Ahn, J. Mun, Y. Y. Lee, M. Kim, N. H. Cho, K. Chang, W. S. Kim, J. Rho and K. Nam, *Nature*, 2018, **556**, 360–365.
9 N. Tian, Z. Y. Zhou, N. F. Yu, L. Y. Wang and S. G. Sun, *J. Am. Chem. Soc.*, 2010, **132**, 7580.
10 J. H. Du, T. Sheng, C. Xiao, N. Tian, J. Xiao, A. Xie, S. Liu, Z. Zhou and S. G. Sun, *Chem. Commun.*, 2017, **22**, 3236–3238.
11 G. R. Guillerm, D. N. Pablo, R. Antonio, P. Alejandro, T. Gloria, G. Jesús, B. Luis, L. Pablo, G. M. Luis, A. P. Mauricio, M. L. Luis, P. R. Ovidio and G. M. Andrés, *Science*, 2017, **358**, 640–644.
12 J. Park, Y. Lee and J. Nam, *Nano Lett.*, 2018, **18**(10), 6475–6482.
13 Y. Li, L. Jiang, Y. Zou, Z. Song and S. Jin, *Appl. Surf. Sci.*, 2021, **540**, 148381.
14 C. Li, K. L. Shuford, M. Chen, E. Lee and S. O. Cho, *ACS Nano*, 2008, **2**, 1760–1769.
15 Y. Lu, H. Zhang, F. Wu, H. Liu and J. Z. Fang, *RSC Adv.*, 2017, **7**, 18601.
16 H. Ahn, H. Lee, K. Jin and K. T. Nam, *J. Mater. Chem. C*, 2013, **1**, 6861.
17 J. D. Padmos, M. L. Personick, Q. Tang, P. N. Duchesne, D. Jiang, C. A. Mirkin and P. Zhang, *Nat. Commun.*, 2015, **6**, 7664.
18 W. Wang, C. Wu, J. Zhu, Y. Han, Y. Fan and Y. Wang, *CrystEngComm*, 2018, **20**, 7631–7636.
19 D. Huo, H. Ding, S. Zhou, J. Li, J. Tao, Y. Ma and Y. Xia, *Nanoscale*, 2018, **10**, 11034.
20 F. Lu, Y. Zhang, L. Zhang, Y. Zhang, J. X. Wang, R. R. Adzic, E. A. Stach and O. Gang, *J. Am. Chem. Soc.*, 2011, **133**, 18074–18077.
21 J. Li, L. Wang, L. Liu, L. Guo, X. Han and Z. Zhang, *Chem. Commun.*, 2010, **46**, 5109–5111.
22 J. W. Hong, S. U. Lee, Y. W. Lee and S. W. Han, *J. Am. Chem. Soc.*, 2012, **134**, 4565.
23 L. Zhang, W. Niu, W. Gao, L. Qi, J. Lai, J. Zhao and G. Xu, *ACS Nano*, 2014, **8**, 5953.
24 W. Niu, Y. Duan, Z. Qing, H. Huang and X. Lu, *J. Am. Chem. Soc.*, 2017, **139**, 5817–5826.
25 L. Zhang, R. Hao, D. Zhang, H. You, Y. Dai, W. Liu and J. Fang, *Anal. Chem.*, 2020, **92**(14), 9838–9846.
26 Y. Li, M. Zhai and H. Xu, *Appl. Surf. Sci.*, 2019, **498**, 143864.
27 H. Yuan, W. Ma, C. Chen, J. Zhao, J. Liu, H. Zhu and X. Gao, *Chem. Mater.*, 2007, **19**, 1592–1600.
28 H. Yuan, W. Ma, C. Chen, H. Zhu, X. Gao and J. Zhao, *J. Phys. Chem. C*, 2011, **115**, 23256–23260.
29 Y. H. Su, S. L. Tu, S. W. Tseng, Y. C. Chang, S. H. Chang and W. M. Zhang, *Nanoscale*, 2010, **2**, 2639–2646.
30 J. Li, J. Zhou, T. Jiang, B. Wang, M. Gu, L. Petti and P. Mormile, *Phys. Chem. Chem. Phys.*, 2014, **16**, 25601–25608.
31 V. Sebastian, S. K. Lee and K. F. Jensen, *Nanoscale*, 2014, **6**, 13228–13235.
32 D. Lee, H. Lee, Y. Jeong, Y. Ahn, G. Nam and Y. Lee, *Adv. Mater.*, 2016, **28**, 9364–9369.
33 A. Pangdam, S. Nootchanat, R. Ishikawa, K. Shinbo, K. Kato, F. Kaneko, C. Thammacharoen, S. Ekgasit and A. Baba, *Phys. Chem. Chem. Phys.*, 2016, **18**, 18500–18506.
34 A. Mathew, P. R. Sajanlal and T. Pradeep, *J. Cryst. Growth*, 2010, **312**, 587–594.
35 Y. Li, M. Zhai and H. Xu, *Appl. Surf. Sci.*, 2019, **498**, 143864.
36 Y. F. Peng, R. Li, X. Sun, G. Wang and Z. Li, *Anal. Chim. Acta*, 2020, **1121**, 17–25.
37 T. Tezcan and C. H. Hsu, *RSC Adv.*, 2020, **10**, 34290.
38 H. Yuan, C. G. Khoury, H. Hwang, C. M. Wilson, G. A. Grant and T. Vo-Dinh, *Nanotechnology*, 2012, **23**, 75102.
39 L. Zhang, R. Hao, D. Zhang, H. You, Y. Dai, W. Liu and J. Fang, *Anal. Chem.*, 2020, **92**(14), 9838–9846.
40 J. Sun, J. Wang, W. Hu, Y. Wang, T. Chou, Q. Zhang, B. Zhang, Z. Yu, Y. Yang, L. Ren and H. Wang, *ACS Appl. Mater. Interfaces*, 2021, **13**, 10778–10795.
41 S. Chakrabarty, S. Maity, D. Yazhini and A. Ghosh, *Langmuir*, 2020, **36**(38), 11255–11261.
42 K. I. Requejo, A. V. Liopo and E. R. Zubarev, *Langmuir*, 2020, **36**, 3758–3769.
43 M. D. Matas, H. G. Edwards, E. E. Lawson, L. Shields and P. York, *J. Mol. Struct.*, 1998, **440**, 97–104.